ARL-TR-9394 • FEB 2022

Direct Numerical Simulation of Particle Transport and Dispersion in Wall-Bounded Turbulent Flows

by Alexandre D Leonelli, Luis G Bravo, and Eckart Meiburg

ARL-TR-9394 ● FEB 2022

Direct Numerical Simulation of Particle Transport and Dispersion in Wall-Bounded Turbulent Flows

Alexandre D Leonelli
Oak Ridge Associated Universities Fellow

Luis G Bravo
Weapons and Materials Research Directorate, DEVCOM Army Research Laboratory

Eckart Meiburg
University of California Santa Barbara

REPORT DOCUMENTATION PAGE			*Form Approved OMB No. 0704-0188*

1. REPORT DATE *(DD-MM-YYYY)*	**2. REPORT TYPE**	**3. DATES COVERED (From - To)**
February 2022	Technical Report	June–December 2021

4. TITLE AND SUBTITLE	**5a. CONTRACT NUMBER**
Direct Numerical Simulation of Particle Transport and Dispersion in Wall-Bounded Turbulent Flows	
	5b. GRANT NUMBER
	5c. PROGRAM ELEMENT NUMBER
6. AUTHOR(S)	**5d. PROJECT NUMBER**
Alexandre D Leonelli, Luis G Bravo, and Eckart Meiburg	
	5e. TASK NUMBER
	5f. WORK UNIT NUMBER
7. PERFORMING ORGANIZATION NAME(S) AND ADDRESS(ES)	**8. PERFORMING ORGANIZATION REPORT NUMBER**
DEVCOM Army Research Laboratory ATTN: FCDD-RLW-VA Aberdeen Proving Ground, MD 21005	ARL-TR-9394
9. SPONSORING/MONITORING AGENCY NAME(S) AND ADDRESS(ES)	**10. SPONSOR/MONITOR'S ACRONYM(S)**
	11. SPONSOR/MONITOR'S REPORT NUMBER(S)

12. DISTRIBUTION/AVAILABILITY STATEMENT

Approved for public release: distribution unlimited.

13. SUPPLEMENTARY NOTES

ORCID ID: Luis Bravo, 0000-0003-1604-9303

14. ABSTRACT

The multiphase wall-bounded turbulence resolving capabilities of particle-laden flows via immersed boundaries (PARTIES), an academic in-house particle-resolving direct numerical simulation code (Biegert et al. 2017; Vowinckel et al. 2019) is validated against Picano et al. (2015). Particle-turbulence interactions in wall-bounded flows is a problem of great importance in order to predict particle transport, aggregation, and deposition for a broad range of engineering applications. In this work, four simulations of turbulent channel flow of dense suspensions are performed. The suspensions comprise neutrally buoyant particles immersed in a Newtonian fluid with volume fractions of $\Phi = \{0, 0.05, 0.1, 0.2\}$. Coupling between the fluid and solid phases is achieved by the Immersed Boundary Method. The mean streamwise fluid velocity, local solid volume fraction, and solid-phase velocity are examined and found to be in good agreement with reference data. PARTIES appears to slightly underestimate the wall shear stress, which may be attributed to a discrepancy in the applied pressure gradient and Reynolds number. Despite the small inconsistencies, PARTIES successfully captures the relevant internal flow physics reported by Picano et al. (2015) and is a promising tool to study particle-laden systems of relevance to the Army.

15. SUBJECT TERMS

turbulence, multiphase flows, direct numerical simulation, DNS, Immersed Boundary Method, Reynolds number

16. SECURITY CLASSIFICATION OF:			**17. LIMITATION OF ABSTRACT**	**18. NUMBER OF PAGES**	**19a. NAME OF RESPONSIBLE PERSON**
					Luis G Bravo
a. REPORT	**b. ABSTRACT**	**c. THIS PAGE**			**19b. TELEPHONE NUMBER (Include area code)**
Unclassified	Unclassified	Unclassified	UU	19	(410) 278-9719

Standard Form 298 (Rev. 8/98)
Prescribed by ANSI Std. Z39.18

Contents

List of Figures	**iv**
List of Tables	**iv**
Acknowledgments	**v**
1. Introduction	**1**
2. Methodology	**3**
2.1 Governing Equations and Computational Method	3
2.2 Setup	4
3. Results	**5**
4. Conclusions	**8**
5. References	**10**
List of Symbols, Abbreviations, and Acronyms	**11**
Distribution List	**12**

List of Figures

Fig. 1 Marine Corps MV-22 operating in brownout conditions 2

Fig. 2 Summary of coupling modes 2

Fig. 3 Snapshots of the streamwise velocity $U_f$for comparison with Fig. 2 in Picano et al. The streamwise velocity nearest the domain boundaries is projected onto the bounding orthogonal planes. For visual clarity, particles are only rendered in half of the domain. 6

Fig. 4 Plane-averaged fluid velocity profiles in outer units a) and inner units b) $U_f^+ = U_f/u_\tau$ and $y^+ = u_\tau/\nu$ where the friction velocity, uτ and fluid kinematic viscosity, ν are defined in Section 2. Solid lines indicate data produced with PARTIES, while dotted lines present the data of Picano et al. The gray dashed line in b) displays the law of the wall $u^+ = \frac{1}{\kappa}\log y^+ + C^+$ with $\kappa = 0.4$ and $C^+ = 5.5$ 7

Fig. 5 a) Plane-averaged local volume fraction. b) Plane-averaged particle streamwise velocity in inner units: $U_p^+ = U_p/u_\tau$. Data from PARTIES (solid lines) and Picano et al. (dotted lines) are displayed.................... 8

List of Tables

Table 1 Summary of simulation parameters. In total, four simulations of varied Φ were performed as validation against Picano et al........................... 5

Acknowledgments

This research was sponsored by the High Performance Computing (HPC) Modernization Program and the HPC Internship Program (HIP) under the supervision of Dr Luis Bravo. I also gratefully acknowledge the support of the DEVCOM ARL and the Department of Defense HPC centers (Engineer Research and Development Center) for use of their HPC systems. Additionally, many thanks to my HIP mentor at DEVCOM ARL Dr Luis Bravo, my PhD advisor Professor Eckart Meiburg, along with the rest of the Vertical Takeoff and Landing Turbine Power Research Team for their guidance, patience, and curiosity.

1. Introduction

The study of multiphase flows is broad, with industrial and military applications such as oil extraction, advanced materials manufacturing, hypersonic flight through ice crystals or dust, sand ingestion by gas-turbine engines and rotorcraft (Jain et al. 2021), flight through volcanic ash and dust clouds (Giehl et al. 2017), and various other pyroclastic and environmental flows. Understanding the dynamics and underlying physics of such flows is critical to developing next-generation capabilities and assessing operational risks.

Describing multiphase flows is nontrivial, as flow characteristics are influenced by properties such as, but not limited to, particle size and shape, volume fraction, solid-to-fluid density ratio, viscosity, agglomeration, and flow speed. While much progress has been made through empirical models, the underlying particle-scale physics responsible for phenomena such as flow modulation, shear thickening/ thinning, clogging, and agglomeration are not well understood. This is partly due to the difficulty of direct observation of the dispersed phase, a difficulty circumvented by particle-resolving simulations. As such, particle-resolving direct numerical simulation (PR-DNS), in which individual particles and their interactions are tracked within the fluid phase, has become increasingly popular. PR-DNS achieves accuracy by directly integrating the fluid and solid equations of motion, though coupling of the two phases is dependent on the application and code capabilities. For low-volume fractions, particles generally do not affect the fluid phase and therefore two-way coupling between the phases is not required. This so-called "one-way" coupled regime is characteristic of the flows such as those found in gas-turbine engines where the volume fraction is on the order of $\Phi \sim 10^{-6}$ (Jain et al. 2021). As the volume fraction increases, such as in extreme brownout events (Fig. 1) or when flying near dense volcanic or soot clouds, the effect of the particles on the fluid can no longer be ignored and complete solid–fluid and solid–solid coupling is needed.

Fig. 1 Marine Corps MV-22 operating in brownout conditions (Harrington 2007)

Particle-laden flows via immersed boundaries (PARTIES), the Meiburg Computational Fluid Dynamic (CFD) Lab's PR-DNS code, achieves this "four-way" coupling via the well-established Immersed Boundary Method (IBM) (Biegert et al. 2017). With the capability of fully resolving individual particles and their influence on both the flow and other particles, PARTIES has been primarily used to study less-energetic environmental flows. PARTIES also has the capability to operate in the one-way coupled regime as demonstrated in a recent study of flocculation in homogeneous isotropic turbulence at volume fractions and flow parameters similar to those seen by external rotorcraft blade tips under brownout conditions (Zhao et al. 2021). A summary of the various coupling modes available in PARTIES is displayed in Fig. 2.

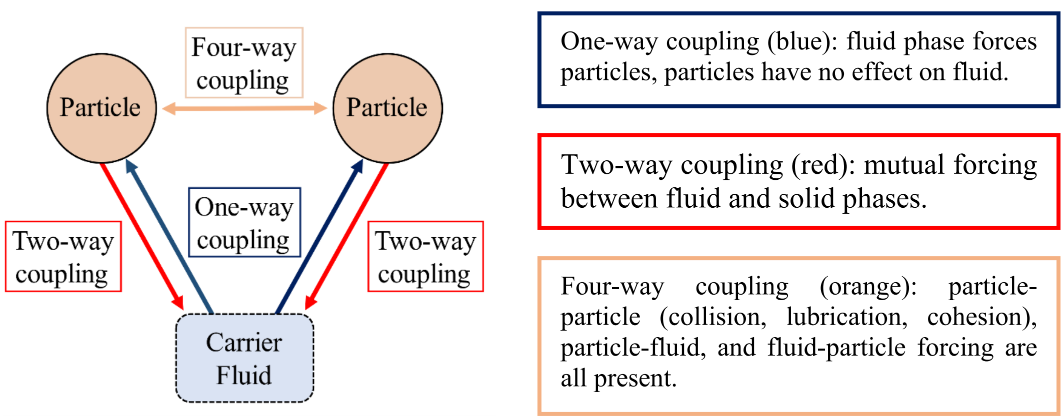

Fig. 2 Summary of coupling modes. Figure adapted from Khare et al. (2015).

Simulations of multiphase turbulence in the four-way coupled regime have not been tractable until recently, and the application of PARTIES to inhomogeneous turbulent flow is novel. As such, the capabilities of PARTIES to operate in this regime are unknown and require validation. The goal of the present work is to investigate these capabilities by validating PARTIES against work performed by

Picano et al. (2015), who use a similar PR-DNS- and IBM-based code to study turbulent channel flow of dense suspensions comprising neutrally buoyant spherical particles dispersed into a Newtonian fluid at various volume fractions. With proper validation, the knowledge gained from one-way PARTIES simulations of homogeneous isotropic turbulence, such as those conducted by Zhao et al. (2021), can be complemented by simulations of inhomogeneous turbulence in both the one-way and four-way coupled regimes. As a result, PARTIES will be capable of better describing flows such as debris ingestion into aircraft engines or the mixing of solutions in materials manufacturing, as examples.

2. Methodology

2.1 Governing Equations and Computational Method

To fully describe the dynamics at such high-volume fractions, the fluid and particle motion must be fully coupled. PARTIES implements an interface-resolving IBM to achieve this coupling. The IBM transfers quantities such as force and velocity between the fluid phase stored on a cubic Eulerian grid and the solid phase the surface of which is described by Lagrangian marker points. Each particle is independently resolved by N_l Lagrangian points, where N_l is dependent on the particle size and grid resolution.

The fluid phase is described by the incompressible Navier–Stokes equation,

$$\nabla \cdot \mathbf{u}_\mathrm{f} = 0\,, \tag{1}$$

$$\frac{\partial \mathbf{u}_f}{\partial \mathrm{t}} + \mathbf{u}_f \cdot \nabla \mathbf{u}_f = -\frac{1}{\rho}\nabla \mathrm{p} + \nu \nabla^2 \mathbf{u}_f + \mathbf{F}_{IBM}\,, \tag{2}$$

where the IBM forcing term $\mathbf{F}_{IBM}$ accounts for the forcing of the fluid by the solid phase. The dynamics of each individual particle are governed by the linear and angular momentum equations

$$m_p \frac{\mathrm{d}\mathbf{u}_p}{\mathrm{d}t} = \underbrace{\oint_{\Gamma_p} \boldsymbol{\tau} \cdot \mathbf{n}\,\mathrm{d}A}_{\mathbf{F}_{h,p}} + \mathrm{V_p}(\rho_\mathrm{p} - \rho_\mathrm{f})\mathrm{g} + \mathbf{F}_{c,p}\,, \tag{3}$$

$$m_p \frac{d\mathbf{u}_p}{dt} = \underbrace{\oint_{\Gamma_p} \mathbf{r} \times (\boldsymbol{\tau} \cdot \mathbf{n})\mathrm{d}A}_{\mathbf{T}_{h,p}} + \mathbf{T}_{c,p}\,. \tag{4}$$

Here the fluid-particle coupling terms $\mathbf{F}_{h,p}$ and $\mathbf{T}_{h,p}$ are again handled by the IBM, while contact, lubrication, and cohesion models are employed, if applicable, for the solid interaction terms $\mathbf{F}_{c,p}$ and $\mathbf{T}_{c,p}$. For a single particle i, the close-range linear and tangential forces due to particle j and wall w are modeled as

$$\mathbf{F}_{c,p} = \sum_{i,i\neq j}^{N_p} \left(\mathbf{F}_{con,ij} + \mathbf{F}_{lub,ij} + \mathbf{F}_{coh,ij} \right) + \mathbf{F}_{con,w} + \mathbf{F}_{lub,w} + \mathbf{F}_{coh,\mathrm{w}} \,, \tag{5}$$

$$\mathbf{T}_{c,p} = \sum_{i,i\neq j}^{N_p} \mathbf{T}_{con,ij} + \mathbf{T}_{con,w} \,, \tag{6}$$

where $\mathbf{F}_{con,ij}$, $\mathbf{F}_{lub,ij}$, and $\mathbf{F}_{coh,ij}$ are the contact, lubrication, and cohesive forces on particle i due to particle j; $\mathbf{F}_{con,w}$, $\mathbf{F}_{lub,w}$, and $\mathbf{F}_{coh,w}$ are the contact, lubrication, and cohesive forces on particle i due to wall w; $\mathbf{T}_{con,ij}$ is the torque on particle i due to particle j; and $\mathbf{T}_{con,w}$ is the torque on particle i due to wall w. The solid interaction models generally take effect once the gap between two solid surfaces is on the order of a grid cell (i.e., once the hydrodynamic forces can no longer be resolved by the IBM and DNS alone). A more detailed discussion and validation of the models employed in PARTIES can be found in Biegert et al. (2017) and Vowinckel et al. (2019).

2.2 Setup

To study and validate the capabilities of PARTIES in simulating wall-bounded turbulent flows, this study performs four simulations of channel flow of suspensions between two infinite parallel plates. In each simulation, one of four suspensions of various $\Phi = 0\text{–}\,0.2$ composed of N_p neutrally buoyant ($\rho_p/\rho_f = 1$) particles of diameter $D = \delta/9$ is considered. The channel is of size $L_x = 6\delta$, $L_y = 2\delta$, and $L_z = 3\delta$ with periodic boundary conditions in the streamwise, x, and spanwise, z, directions, and no-slip conditions are enforced at the walls located at $y = 0$ and $y = 2\delta$. The same cubic grid, $N_x = 864$, $N_y = 288$, $N_z = 432$, employed by Picano et al. (2015) is used to discretize the domain. In each case, a constant pressure gradient corresponding to a bulk streamwise velocity of $U_0 = 1$ is maintained across the channel. A bulk Reynolds number $Re_b = U_0\delta/\nu = 2800$ is defined with ν, the kinematic viscosity of the fluid phase. For the unladen case, the bulk Reynolds number as well as the friction Reynolds number $Re_\tau = u_\tau\delta/\nu = 180$, based on the friction velocity $u_\tau = \sqrt{\tau_w/\rho}$ and wall shear stress $\tau_w = \rho\nu\partial U_f/\partial y|_{y=0}$, correspond to the classical investigation into turbulent channel flow performed by Kim et al. (1987). For the suspensions, an effective viscosity ν_e is estimated using the Eilers fit $\nu_e/\nu = [1 + 1.25\Phi/(1 - \Phi/0.6)]^2$

(Picano et al. 2015). The effective viscosity is used to calculate an effective Reynolds number $Re_e = U_0\delta/\nu_e$ and effective wall shear stress $\tau_{w,e} = \rho\nu_e \partial U_f/\partial y|_{y=0}$ for each volume fraction. A summary of simulation parameters can be found in Table 1.

Table 1 Summary of simulation parameters. In total, four simulations of varied Φ were performed as validation against Picano et al. (2015)

$\boldsymbol{\Phi}$	$\mathbf{0}$	$\mathbf{0.05}$	$\mathbf{0.1}$	$\mathbf{0.2}$
$\boldsymbol{N_p}$	0	2506	5012	10024
$\boldsymbol{Re_\delta}$	2800			
$\boldsymbol{L_x \times L_y \times L_z}$	$6\delta \times 2\delta \times 3\delta$			
$\boldsymbol{N_x \times N_y \times N_z}$	$864 \times 288 \times 432$			
$\boldsymbol{N_{cpu}}$ **(ONYX)**	3080			

A laminar Poiseuille flow laden with the appropriate number of randomly distributed particles serves as the initial condition. Transition occurs due to perturbations introduced by the particles. For the unladen case, the flow is initially seeded with $N_p = 501$ ($\Phi = 0.01$). Once the flow is turbulent, the particles are removed, and the simulation is continued until the remnant flow structures associated with the solid phase vanish. For all cases, data are collected once a statistically stationary state identified by a quasi-periodic total kinetic energy is reached (Kim et al. 1987). The simulations were run on the Engineer Research and Development Center Department of Defense Supercomputing Resource Center–maintained ONYX Cray $XC40/50$ system using 3080 cores for approximately 5×10^5 central processing unit hours.

3. Results

The instantaneous streamwise velocity fields for each of the four volume fractions in consideration are visualized in Fig. 3. The lower plane displays the streamwise velocity in the boundary layer at the first grid point above the wall. Streaks, a classical characteristic of wall-bounded turbulence (Kline et al. 1967), are expectedly present in the boundary layer. The streaks are most clearly defined in the $\Phi = 0$ case and, as reported by Picano et al. (2015), become wider and noisier at higher volume fractions.

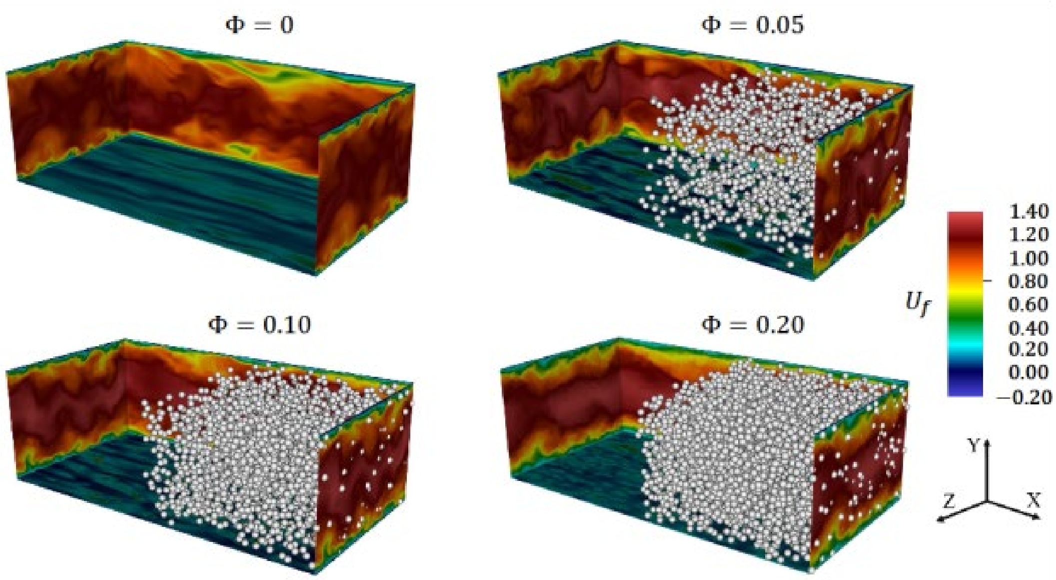

Fig. 3 Snapshots of the streamwise velocity U_f for comparison with Fig. 2 in Picano et al. (2015). The streamwise velocity nearest the domain boundaries is projected onto the bounding orthogonal planes. For visual clarity, particles are only rendered in half of the domain.

To avoid reiterating the previous work and remain focused on the goal of validation, the discussion is limited to comparisons of statistics and not physical explanations of the phenomena. For an overview of the phenomena, see Picano et al. (2015). Unlike Picano et al., the results presented for PARTIES are not time averaged. Before the present work, PARTIES had not been applied to inhomogeneous turbulent flows and, therefore, much of the input/output and postprocessing capabilities required to study such flows are still in development. The lack of time averaging manifests as noise and data that might be slightly perturbed from the true mean. This is addressed explicitly in the text when relevant. Note that statistics pertaining to the fluid phase are calculated using only points located outside of the particle volumes, which further decrease the sample size.

A comparison of the xz-plane-averaged fluid velocity profiles is presented in Fig. 4. Figure 4a shows the average streamwise velocity in outer units, U_f, for half of the channel. PARTIES successfully captures the classical flattening of the turbulent Poiseuille flow profile in the $\Phi = 0$ case as well as the return to a more parabolic profile as the volume fraction increases. Fluctuations due to the lack of time averaging are most clearly present in the $\Phi = 0.2$ case; however, these fluctuations do not detract from the phenomenology. PARTIES displays a larger spread in the streamwise velocity profiles; the two-phase velocity profiles are slightly suppressed near the wall and overestimate the centerline velocity, while the opposite is true for the single-phase simulation. These inconsistencies are likely due to either a variability of approximately 10% in U_0 (and thus Re_δ) due to discrepancies involving the imposed pressure gradient and a lack of time averaging. The disparity in mean streamwise velocity profiles may also be attributed to grid resolution; however, both PARTIES and the code used by Picano et al. (2015) maintain second-order accuracy in space and use identical grids. The velocity profiles in inner units, $U_f^+ = U_f/u_\tau$ and $y^+ = yu_\tau/\nu$, are reported on a log-linear scale in Fig. 4b. The well-established law of the wall is overlaid onto the data, demonstrating the success of both studies at capturing the inner region of the flow in the single-phase case.

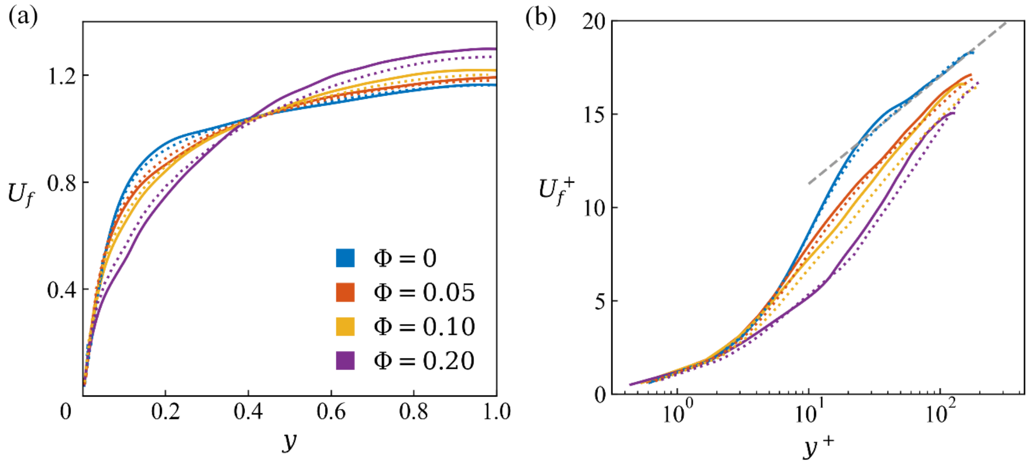

Fig. 4 Plane-averaged fluid velocity profiles in outer units a) and inner units b) $U_f^+ = U_f/u_\tau$ and $y^+ = yu_\tau/\nu$ where the friction velocity, u_τ and fluid kinematic viscosity, ν are defined in Section 2. Solid lines indicate data produced with PARTIES, while dotted lines present the data of Picano et al. (2015). The gray dashed line in b) displays the law of the wall $u^+ = \frac{1}{\kappa} log\, y^+ + C^+$ with $\kappa = 0.4$ and $C^+ = 5.5$.

Figure 5a shows the local volume fraction in outer units, while the mean streamwise velocity of the solid phase is reported in Fig. 5b. Disregarding the increased noise (again due to the lack of time averaging), both sets of data for the local volume fraction are in good agreement. Interestingly, despite the consistency in the spatial distribution, the streamwise particle velocities differ near the wall. In accordance with Picano et al. (2015), this suggests that the particle distribution, particularly the formation of a particle layer at the wall (seen as a near-wall local maximum in Fig. 5a), can be attributed to the channel geometry rather than flow characteristics. Several issues are present in the reporting of the mean particle velocity. The profiles suggested by PARTIES appear shifted to the left of the data of Picano et al., indicating that PARTIES underestimates the wall shear stress τ_w (recall $y^+ \sim \sqrt{\tau_w}$). Better agreement in both the solid and liquid phase velocities (Figs. 4b and 5b) is achieved when τ_w is increased by 5%; however, this is an arbitrary correction and does not account for the discrepancy seen near the wall. This near-wall region, $y^+ < 10 \approx R^+$, displays the mean velocity of the near-wall particle layer. The difference is not present in the $\Phi = 0.20$ case, which suggests that the offset might be due to the particle sample size in the region. Indeed, the number of particles present in the region within one particle diameter of the wall is $N_{0.05} = 78$, $N_{0.10} = 156$, and $N_{0.20} = 312$ for $\Phi = 0.05$, $\Phi = 0.10$, and $\Phi = 0.20$, respectively. Thus, the lack of time averaging is especially detrimental to the lower volume fraction cases. Note this difference is only present in the solid phase velocity; the fluid phase velocities are in relatively good agreement near the wall (see Fig. 4b). Further investigation with time averaging and a corrected τ_w is needed before conclusions can be made regarding the ability of PARTIES to capture these near-wall particle velocities. If the discrepancy in near-wall particle velocity persists, examination of the particle-wall collision models might be required.

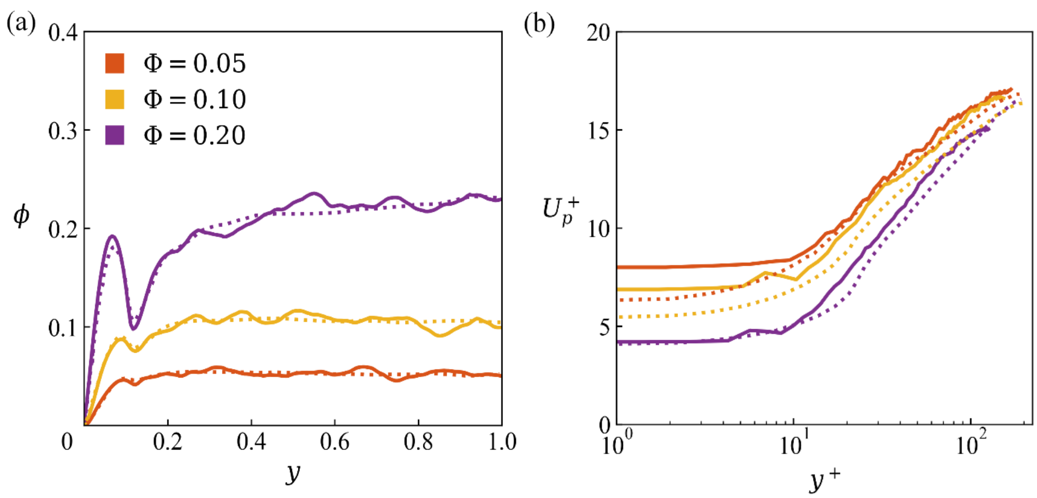

Fig. 5 a) Plane-averaged local volume fraction. b) Plane-averaged particle streamwise velocity in inner units: $U_p^+ = U_p/u_\tau$. Data from PARTIES (solid lines) and Picano et al. (2015) (dotted lines) are displayed.

4. Conclusions

The multiphase turbulence-resolving capabilities of PARTIES, an in-house IBM based PR-DNS code, is validated against the data of Picano et al. (2015). Four simulations of turbulent channel flow ($Re_\delta = U_0\delta/\nu = 2800$) of suspensions with volume fractions in the range of $\Phi = 0$-0.2 are performed and compared with the referenced data.

While PARTIES captures much of the phenomenology presented in Picano et al., small discrepancies are present. Most significant is an apparent underestimation of the wall shear stress $\tau_w = \rho\nu_e \partial U_f/\partial y|_{y=0}$ and overestimation of the solid-phase near-wall velocity. These statistics might become consistent with time averaging and improved accuracy in the imposed pressure gradient. Time averaging is expected to reduce noise and skew the data toward the "true" statistical mean, while an improvement in the pressure gradient will reduce variability in the desired constant value of the bulk streamwise velocity, $U_0 = 1$. If inaccuracy persists, an increased grid resolution may be required to capture the near-wall dynamics.

Despite these deviations, PARTIES appears to be nearly ready for use in further studies in multiphase wall-bounded turbulent flows. Possible future investigations include studies of lower volume fractions, such as those seen in gas turbine engines during brownout conditions, or materials development, flocculation dynamics of cohesive particles, and rheology of polydisperse suspensions. Additionally, much work is being done to bring machine-learning-based reduced order models to PR-DNS simulations (He and Tafti 2019; Moore and Balachandar 2019)—a capability that will likely be introduced to PARTIES in the near future, allowing for novel machine-learning-supported multiphase turbulence simulations.

5. References

Biegert E, Vowinckel B, Meiburg E. A collision model for grain-resolving simulations of flows over dense, mobile, polydisperse granular sediment beds. J Comput Phys. 2017 July;340:105–127.

Giehl C, Brooker RA, Marxer H, Nowak M. An experimental simulation of volcanic ash deposition in gas turbines and implications for jet engine safety. Chem Geol. 2017 June;461:160–170.

Harrington, WA. Helicopter dustcloud. Photograph. Eglin Air Force Base; 2007. https://www.eglin.af.mil/News/Photos/igphoto/2000513040/.

He L, Danesh KT. Supervised machine learning approach for predicting variable drag forces on spherical particles in suspension. Powder Tech. 2019 Mar;345:379–389.

Jain N, Le Moine A, Chaussonnet G, Flatau A, Bravo L, Ghoshal A, Walock MJ, Murugan M, Khare P. A critical review of physical models in high temperature multiphase dynamics: turbulent transport and particle-wall interactions. Appl Mech Rev. 2021;73(4):040801.

Khare P, Wang S, Yang V. Modeling of finite-size droplets and particles in multiphase flows. Chinese J Aeronaut. 2015;28(4):974–982.

Kim J, Moin P, Moser R. Turbulence statistics in fully developed channel flow at low Reynolds number. J Fluid Mech. 1987 Apr;177:133–166.

Kline SJ, Reynolds WC, Schraub FA, Runstadler PW. The structure of turbulent boundary layers. J Fluid Mech. 1967;30(4):741–773.

Moore WC, Balachandar S. Lagrangian investigation of pseudo-turbulence in multiphase flow using superposable wakes. Phys Rev Fluids. 2019;4(11):114301.

Picano F, Breugem W-P, Brandt L. Turbulent channel flow of dense suspensions of neutrally buoyant spheres. J Fluid Mech. 2015 Jan;764:463–487.

Vowinckel B, Withers J, Luzzatto-Fegiz P, Meiburg E. Settling of cohesive sediment: particle-resolved simulations. J Fluid Mech. 2019 Jan;858:5–44.

Zhao K, Pomes F, Vowinckel B, Hsu T-J, Bai B, Meiburg E. Flocculation of suspended cohesive particles in homogeneous isotropic turbulence. J Fluid Mech. 2021 Aug;921:A17.

List of Symbols, Abbreviations, and Acronyms

ARL	Army Research Laboratory
CFD	computational fluid dynamics
DEVCOM	US Army Combat Capabilities Development Command
DNS	direct numerical simulation
HPC	High Performance Computing
HIP	HPC Internship Program
IBM	Immersed Boundary Method
PARTIES	particle-laden flows via immersed boundaries
PR-DNS	particle resolving direct numerical simulation

1 (PDF)	DEFENSE TECHNICAL INFORMATION CTR DTIC OCA
1 (PDF)	DEVCOM ARL FCDD RLD DCI TECH LIB
3 (PDF)	DEVCOM ARL FCDD RLW VA L BRAVO A GHOSHAL M MURUGAN
1 (PDF)	UNIV OF CALIFORNIA SANTA BARBARA FE MEIBURG
1 (PDF)	UNIV OF CALIFORNIA BERKELEY P KHARE
1 (PDF)	UNIV OF MARYLAND A FLATAU
1 (PDF)	DOD HPCMP OFFICE LP DAVIS
1 (PDF)	NIST SM SU